

Fluorinated Mesoporous Silica Nanoparticles for Binuclear Probes in H and F Magnetic Resonance Imaging

Meryem Bouchoucha, Ruud B. van Heeswijk, Yves Gossuin, Freddy Kleitz, and Marc-André Fortin

Langmuir, **Just Accepted Manuscript** • DOI: 10.1021/acs.langmuir.7b01792 • Publication Date (Web): 04 Sep 2017

Downloaded from <http://pubs.acs.org> on September 4, 2017

Just Accepted

“Just Accepted” manuscripts have been peer-reviewed and accepted for publication. They are posted online prior to technical editing, formatting for publication and author proofing. The American Chemical Society provides “Just Accepted” as a free service to the research community to expedite the dissemination of scientific material as soon as possible after acceptance. “Just Accepted” manuscripts appear in full in PDF format accompanied by an HTML abstract. “Just Accepted” manuscripts have been fully peer reviewed, but should not be considered the official version of record. They are accessible to all readers and citable by the Digital Object Identifier (DOI®). “Just Accepted” is an optional service offered to authors. Therefore, the “Just Accepted” Web site may not include all articles that will be published in the journal. After a manuscript is technically edited and formatted, it will be removed from the “Just Accepted” Web site and published as an ASAP article. Note that technical editing may introduce minor changes to the manuscript text and/or graphics which could affect content, and all legal disclaimers and ethical guidelines that apply to the journal pertain. ACS cannot be held responsible for errors or consequences arising from the use of information contained in these “Just Accepted” manuscripts.

1
2
3 **Fluorinated Mesoporous Silica Nanoparticles for Binuclear Probes in ¹H**
4
5 **and ¹⁹F Magnetic Resonance Imaging**
6
7

8
9 Meryem Bouchoucha^{‡,§,⊥}, Ruud B. van Heeswijk⁺, Yves Gossuin^{||}, Freddy Kleitz^{‡,⊥}, Marc-
10
11 André Fortin^{§,⊥,*}
12

13
14
15 [‡] Department of Chemistry, Université Laval, Québec (QC), G1V 0A6, Canada. Québec (QC),
16
17 G1V 0A6, Canada.
18

19
20 [§] Department of Mining, Metallurgy and Materials Engineering, Université Laval and Centre
21
22 de recherche du centre hospitalier universitaire de Québec (CR-CHUQ), axe Médecine
23
24 régénératrice, Québec (QC), G1L 3L5, Canada.
25

26
27 [⊥] Centre de recherche sur les matériaux avancés (CERMA), Université Laval, Québec (QC),
28
29 G1V 0A6, Canada.
30

31
32 ⁺ Department of Radiology, Centre Hospitalier Universitaire Vaudois (CHUV), 1011
33
34 Lausanne, Switzerland.
35

36
37 ^{||} Service de physique expérimentale et biologique, Université de Mons, 24 avenue du Champ-
38
39 de-Mars, 7000 Mons, Belgium.
40

41
42 ^{*} Corresponding author
43

44 **Keywords:** mesoporous silica nanoparticles, fluorinated silica, fluorine probes in MRI, ¹⁹F
45
46 MRI, nuclear magnetic relaxation dispersion, relaxivity of gadolinium contrast agents,
47
48 relaxivity of fluorine probes.
49
50
51
52
53
54
55
56
57
58
59
60

1
2
3
4
5
6 **Abstract:** The development of molecular and cellular magnetic resonance imaging
7
8 procedures has always represented a challenge due to the fact that conventional MRI contrast
9
10 agents are not directly detected in vivo; in proton MRI (e.g. with the nucleus ^1H), their local
11
12 concentration is measured through the effect they exert on the signal of hydrogen protons
13
14 present in their immediate vicinity. Because the contrast effects generated by conventional
15
16 MRI probes superpose to and can often impede the anatomical information contained in ^1H
17
18 MRI images, new probes based on another nucleus than ^1H , are being developed. In this
19
20 study, we report on the development of fluorinated mesoporous silica nanoparticles (MSNs),
21
22 which could represent an interesting dual probe allowing two MR imaging modes: ^1H for
23
24 high-resolution anatomical information, and ^{19}F for the detection of MSNs used as drug
25
26 delivery agents. MSNs were synthesised and covalently functionalized either with
27
28 fluorosilane (FMSNs) or polyfluorosiloxane (polyFMSNs) to enable their detection in ^{19}F
29
30 MRI. Then, gadolinium chelates were grafted on the particles to enhance their detectability in
31
32 ^1H -MRI. The physico-chemical, textural and relaxometric properties (^1H and ^{19}F relaxation
33
34 times) of the nanoparticles were measured and compared. The ^{19}F relaxation properties were
35
36 found to be dependent on the concentration of fluorine; they were also highly sensitive to the
37
38 presence of gadolinium. The shortest relaxation times were obtained with polyFMSNs. At
39
40 clinical magnetic field strengths, high ^1H relaxivities and low relaxometric ratios ($r_2/r_1 = 1.45$;
41
42 2.2 for nanoparticles entrapped in hydrogel) were found for both nanoparticle systems.
43
44 Finally, the visibility of both systems were confirmed in ^1H , and the detectability of
45
46 polyFMSNs was confirmed in ^{19}F MRI. This physico-chemical and relaxometric study opens
47
48 the door to applications of FMSNs as theranostic materials allowing dual MRI (^1H and ^{19}F).
49
50
51
52
53
54
55
56
57
58
59
60

Introduction

Mesoporous silica nanoparticles (MSNs) figure among the most significant advances nanotechnology has made in the last three decades.¹ These materials have been explored and exploited for their numerous applications in catalysis,² analytical extraction,³ sensing,^{4, 5} optics,⁶ drug delivery⁷ and bioimaging.⁸ The grafting of fluorinated compounds at the surface of MSNs could lead to innovative materials in chromatography and molecular separation,⁹ as biosensors,¹⁰ as hydrophobic coatings for optical applications¹¹⁻¹³ as well as for catalytical systems¹⁴. In fact, one of the greatest assets of MSNs is the ability to functionalize both their external and their inner surface with different functional groups. To achieve this goal with fluorinated compounds, new grafting procedures must be developed. In fact, biomedical imaging is one of the areas that could benefit the most from MSNs fluorinated products; however, biomedical MSNs must be surface-treated in a certain way as to preserve their hydrophilicity and their colloidal stability. This represents a certain challenge that must be addressed in a systematic and comprehensive study.

Fluorinated nanoparticles can be detected by ¹⁹F-magnetic resonance imaging (MRI), and this innovative bioimaging modality had lead to the emergence of innovative medical procedures (e.g. diagnostic and theranostics).¹⁵ Compared to the other clinical molecular imaging techniques mainly based on the injection of radioisotopes (e.g. positron emission tomography), MRI does not rely on ionizing radiation. It is a non-invasive, whole-body diagnostic tool that is widely used both in pre-clinical and in clinical procedures. MRI scanners usually detect the signal from hydrogen protons (¹H): the most important advantage of ¹H MRI is the capacity to generate anatomical images from the strong hydrogen contents of the human body. However, the ¹⁹F nucleus can also be very sensitively detected by MRI; it has a 100% natural abundance and it resonates at a frequency corresponding to 94% of that of

1
2
3 ^1H . Only a slight change in the radiofrequency wave used to excite the ^1H nucleus is
4
5 necessary to activate the detection of signal in ^{19}F -MRI. Only limited investment in the
6
7 hardware of MRI systems currently installed in hospitals and clinics would be necessary to
8
9 endow the current infrastructure with a dual $^1\text{H}/^{19}\text{F}$ detection capacity. In fact, the interest of
10
11 the medical imaging community for the potential of ^{19}F -MRI has been growing in the past few
12
13 years.
14

15
16 Because the biological tissues contain only traces of fluorine, probes made of ^{19}F
17
18 could be detected in MRI at a potentially very strong signal-to background ratio.¹⁶ The
19
20 detected signal can be directly correlated with the concentration of ^{19}F probes accumulated in
21
22 specific organs. This appears significantly different to the usual detection of ^1H with MRI,
23
24 which is generally used generate most clinical MRI anatomical images based on the very
25
26 strong signal of protons in the mobile water molecules of biological tissues (^1H instead of ^{19}F
27
28 as the signal nucleus). Hence, ^{19}F -based imaging probes detected with ^{19}F -MRI, and
29
30 superposed onto ^1H -MRI anatomical maps, could provide strategy similar to that of other
31
32 imaging procedures where an anatomical modality (e.g. MRI or CT) is coupled with a
33
34 molecular one based on the high-sensitivity detection of radioactive probes (e.g. positron
35
36 emission or single-photon emission computed tomography – PET and SPECT). In the case of
37
38 dual ^{19}F - ^1H -MRI, the major advantage would rely on the possibility to perform totally
39
40 ionizing radiation-free imaging sequences. Therefore, fluorine MRI could be used as an
41
42 alternative to radioactive tracers in certain quantitative biodistribution studies. The
43
44 development of probes containing enough fluorine to reach detectability in ^{19}F -MRI, is the
45
46 highest challenge in this field. Therefore, there is a need at the moment to explore different
47
48 synthetic routes enabling the production of nanoparticle-based imaging probes having
49
50 multiple fluorine groups grafted either at their surface, or within their core.
51
52
53
54
55
56
57
58
59
60

1
2
3 During the past few decades, imaging probes based on ^{19}F (non-silica) have already
4 been developed for cell tracking and inflammation imaging.¹⁷ These probes were formulated
5 from perfluorocarbon molecules (PFCs) such as perfluoro-crown-ether ($\text{C}_x\text{F}_y\text{O}_z$) and C_xF_y ,
6 due to their high content in fluorine atoms.^{17, 18} Unfortunately, perfluorocarbon formulations
7 made of nanoemulsions and micelles have several drawbacks such as low stability, limited
8 aqueous dispersibility and restricted functionalization capacity.¹⁹ In addition to this, the
9 molecular detection of PFC probes in fluorine-MRI is much less sensitive than the detection
10 of radioisotopes in SPECT and PET imaging; in cell tracking procedures, it requires the
11 supersaturation of cells by the PFC contrast agent, often to the limits of cell viability.²⁰
12
13
14
15
16
17
18
19
20
21
22
23
24

25 Recently, the encapsulation of perfluorocarbons in MSNs has been suggested as a
26 strategy to develop an improved generation of fluorinated probes. Perfluorocarbons, either in
27 the form of C_6F_6 or perfluoro-crown-ether molecules, were trapped either in the pores of
28 MSNs, or encapsulated in the core of “core-MSN-shell” systems.²¹⁻²³ The properties of these
29 ^{19}F MRI-traceable nanocarriers appeared promising; however, the fluorine compounds were
30 found prone to diffuse through the pores of the MSN, as observed for small perfluorocarbon
31 molecules (e.g., C_6F_6).²¹ To avoid this undesirable leaching of fluorine groups from the
32 surface of silica materials, it is necessary to graft the fluorine probes with covalent bonds.
33
34
35
36
37
38
39
40
41
42
43
44

45 Another promising aspect of fluorine-grafted MSNs that has not been explored is the
46 development of dual ^{19}F and ^1H MR imaging probes. Paramagnetic elements such as
47 gadolinium (Gd), chelated in small molecules such as diethylenetriaminopentaacetic-acid
48 (Gd-DTPA), can be attached at the surface of MSN. The strong decrease in ^1H longitudinal
49 relaxation times observed in the labeled nanoparticles, enable their efficient imaging in T_1 -
50 weighted ^1H -MRI. Hence, paramagnetic chelates grafted at the surface of MSNs, allows the
51
52
53
54
55
56
57
58
59
60

1
2
3 production of imaging probes that induce a strong "positive" contrast enhancement effect.^{24,25}
4
5 Then, as a second sequential radiological step, the concentration of MSN probes could be
6
7 quantified by ¹⁹F-MRI (molecular imaging modality). To the best of our knowledge, there has
8
9 been no report until now, reporting on the potential of MSN for dual ¹H and ¹⁹F MRI
10
11 procedures.
12

13
14 In this study, mesoporous silica nanoparticles (MSNs; MCM-48-type) were
15
16 synthesised and functionalized with fluorine-containing molecules (fluorosilane and
17
18 fluorosiloxane) and with gadolinium chelates (Gd-DTPA). In both cases, the molecules were
19
20 covalently grafted at the surface of MSNs. The nanoparticles were thoroughly characterized
21
22 and their colloidal stability, assessed by dynamic light scattering (DLS). The relaxometric
23
24 properties of the nanoparticles for ¹⁹F and in ¹H MRI imaging, were measured. The ¹⁹F
25
26 relaxometric performance of fluorosilane-nanoparticles (FMSNs) was also compared to that
27
28 of polyfluorosiloxane-nanoparticles (polyFMSNs). In addition, their ¹H relaxometric
29
30 performance was measured in different media (water and hydrogel) and at various magnetic
31
32 field strengths. Finally, the suspensions of nanoparticles were imaged by ¹H and ¹⁹F MRI (*in*
33
34 *vitro*).
35
36
37
38
39
40
41
42
43
44
45
46
47
48
49
50
51
52
53
54
55
56
57
58
59
60

EXPERIMENTAL SECTION

1) Materials

Tetraethylorthosilicate (TEOS, 98%), Pluronic F127 (EO₁₀₆PO₇₀EO₁₀₆, BioReagent), n-cetyltrimethylammonium bromide (CTAB, 99%), (3-aminopropyl)triethoxysilane (APTES) and diethylenetriaminepentaacetic dianhydride (DTPA dianhydride, 98%) were from Sigma Aldrich (Canada). Dimethoxy-methyl(3,3,3-trifluoropropyl)silane (98%) and Poly(methyl-3,3,3-trifluoropropylsiloxane) were from Gelest (USA).

2) Synthesis of Functionalized Mesoporous Silica Nanoparticles

MCM-48 MSN synthesis: MCM-48-type mesoporous silica nanoparticles were synthesized as reported in the literature.^{26, 27} In brief, CTAB and F127 were dissolved in 298 mL of H₂O/NH₃/EtOH (NH₄OH(aq) 2.9 wt%)/EtOH = 2.5/1 (v/v)). Then, TEOS (3.86 mL) was added over a period of 1 minute, at room temperature (RT) and under a high stirring rate (1000 rpm). Then, the reaction mixture was aged 24 h in static conditions (air, RT). The resulting product was collected by centrifugation, washed twice with water (250 mL), and dried overnight in air at 65°C. Finally, the product was calcined (air, 550°C, 1°C/min, 5h).

DTPA grafting: DTPA molecules were selectively grafted at the outer surface of MSNs as previously reported.²⁴ DTPA dianhydride (65 mg) was dissolved in anhydrous DMSO (at RT, 2 h stirring and 15 min sonication). Then, APTES (55 µL) was added dropwise and the mixture was stirred overnight at RT, and under N₂. The DTPA-silane solution was added to a suspension of nanoparticles (1 g in 170 mL of dry toluene) and the mixture was stirred overnight at RT and under inert gas. The nanoparticles were then centrifuged (10000 rpm for 15 min at least), washed twice with ethanol, once with water, once with acetone and finally dried at 50 °C. The weight percentage of DTPA grafted on the nanoparticles was measured by thermogravimetric analysis (TGA).

1
2
3 **Grafting of fluorosilane:** Fluorosilane molecules (dimethoxy-methyl(3,3,3-
4 trifluoropropyl)silane) were used to graft fluorinated moieties at the surface of MSNs. MSN-
5 DTPA nanoparticles (1 g) were suspended in dry toluene (170 mL). Fluorosilane (5 mL of
6 high purity commercial dimethoxy-methyl(3,3,3-trifluoropropyl)silane solution, 98%) was
7 added to the nanoparticles suspension under inert gas. The mixture was refluxed overnight at
8 110 °C. The functionalized nanoparticles were then centrifuged (10000 rpm for 15 min at
9 least), washed three times with ethanol, once with acetone and finally dried at 50 °C. The
10 w/w percentage of grafted fluorosilane was measured by TGA.
11
12
13
14
15
16
17
18
19

20 **Grafting of polyfluorosiloxane:** Polyfluorosiloxane macromolecules (poly(methyl-
21 3,3,3-trifluoropropylsiloxane), $M_n = 2400$ Da) were also used as a source of fluorine, and the
22 grafting procedure was inspired from previous work.⁹ Briefly, 400 mL of a dichloromethane
23 solution containing 12.5% (w/v) of polyfluorosiloxane, was added to 200 mg of MSNs. The
24 MSNs were previously outgassed at 120 °C overnight. This mixture was slowly stirred at
25 room temperature for 3 h, and then placed in a fume hood at room temperature for
26 evaporation of the dichloromethane (for 1 week at least). Then, the nanoparticles were
27 thermally-treated in a tubular oven under a nitrogen atmosphere (at 200 °C for 12 h) to ensure
28 the immobilization of polyfluorosiloxane molecules onto the silica surface. Then, the
29 nanoparticles were washed twice with dichloromethane, twice with ethanol, once with acetone
30 and finally dried at 50 °C. The w/w percentage of polyfluorosiloxane grafted on the particles
31 was measured by TGA.
32
33
34
35
36
37
38
39
40
41
42
43
44
45
46

47 **PEG Grafting:** PEG-silane (20 kDa) was dissolved in dry toluene under N₂ reflux (0.5
48 mg mL⁻¹). Then, the PEG-silane solution was added to the suspension of calcined
49 nanoparticles (500 mg in 100 mL dry toluene) and the final suspension was refluxed under N₂
50 overnight at 110 °C. After centrifugation (7500G, 10 min), the product was washed twice
51
52
53
54
55
56
57
58
59
60

1
2
3 with EtOH 95%, once with water, and 50 °C. The w/w percentage of grafted PEG was
4
5 measured by TGA.
6

7 **3) Physicochemical characterization**

8
9 *Nitrogen physisorption analysis:* Nitrogen physisorption measurements were
10 performed at −196 °C with an Autosorb iQ2 (Quantachrome Instruments, Boynton Beach,
11 USA). Before the sorption measurements, the samples were outgassed under vacuum at 200
12 °C for 12 h (for pure MSNs) or 80 °C for 10 h (for functionalized MSNs). The surface area
13 (S_{BET}) was determined using the BET equation in the range $0.05 \geq P/P_0 \geq 0.20$, and the total
14 pore volume was measured at $P/P_0 = 0.95$. The diameter of the pores was estimated using
15 methods from the non-local density functional theory (NLDFT), more specifically by
16 applying an adsorption branch model that considers N_2 sorption at −196 °C for silica with a
17 cylindrical pore geometry.²⁸
18
19

20
21 *Thermogravimetric analysis (TGA):* Measurements were performed using a Netzsch
22 STA 449C thermogravimetric analyzer (airflow of 20 mL/min; heating rate = 10 °C/min;
23 heating range of 35 to 700 °C). The total mass percentage of amine and DTPA groups grafted
24 at the surface of MSNs, was calculated based on the mass loss observed between 180 °C and
25 630 °C. These calculation parameters exclude the mass relative to residual solvent (e.g.,
26 physisorbed water). For the measurement of water adsorption, pure and F-modified silica
27 nanoparticles were suspended in water before the measurements, then dried overnight at 50
28 °C followed by TGA measurements. The percentage of water physisorbed on the
29 nanoparticles was calculated from the mass loss observed between 50 °C and 110 °C for F-
30 modified MSNs, and between 50 °C and 140 °C for pure MSNs.
31
32

33
34 *TEM size analysis:* The nanoparticles were suspended in water and 5 μL of the fluid
35 was deposited on a carbon-coated copper grid and dried for at least 24 h. Images were taken
36 with a JEM-1230 TEM at an accelerating voltage of 80 kV. Particle size distributions were
37
38
39
40
41
42
43
44
45
46
47
48
49
50
51

1
2
3 calculated by ImageJ, based on a sample of at least 500 particles, from different images taken
4
5 over different quartiles.
6

7 **Dynamic light scattering:** The hydrodynamic diameter of the nanoparticles was
8
9 measured by dynamic light scattering (DLS) using a Malvern DTS Nano zetasizer 173° (T =
10
11 25 °C, equilibration time set to 3 min; 3 measurements taken on each sample; only quality
12
13 criteria data accepted as valid results).
14

15
16 **NMR general characterization:** Solid-state magic-angle spinning (MAS) nuclear
17
18 magnetic resonance (NMR) spectra were obtained on a Bruker DRX300 MHz NMR
19
20 spectrometer. The 75.4 MHz ¹³C CP-MAS, the 282.2 MHz ¹⁹F MAS and the 59.6 MHz ²⁹Si
21
22 MAS NMR spectra were obtained using a 4 mm rotor spinning at 10 kHz. The chemical shifts
23
24 are reported in ppm relative to adamantane for ¹³C, to trifluoroacetic acid (TFA) for ¹⁹F and to
25
26 tetramethylsilane (TMS) for ²⁹Si.
27
28

29
30 **¹H relaxation analysis and relaxometric properties measurement:** 400 µL of Gd-
31
32 labeled nanoparticles suspensions were pipetted into in 6.0 mm NMR tubes. Longitudinal and
33
34 transversal relaxation times (T_1 and T_2) were measured with a TD-NMR relaxometer (Bruker
35
36 Minispec 60 mq, 60 MHz, 37 °C). The concentration of Gd in each suspension was precisely
37
38 measured by ICP-MS after an optimal digestion procedure in HNO₃ and hydrogen peroxide,
39
40 in order to leach all Gd³⁺ ions from the silica matrix. Relaxation rates ($1/T_1$ and $1/T_2$) were
41
42 plotted against Gd concentration values, and relaxivities (r_1 and r_2) were calculated from the
43
44 slope of these curves. **NMRD profiles:** Nuclear magnetic relaxation dispersion (NMRD)
45
46 profiles (T_1) of aqueous suspensions were measured from 0.015 to 40 MHz with a Spinmaster
47
48 fast field cycling relaxometer (STELAR, Mede, Italy) at 37 °C, using 600 mL of the
49
50 nanoparticles suspensions. Then, longitudinal and transverse relaxation times (T_1 and T_2) were
51
52 measured with Bruker MiniSpec relaxometers (20 and 60 MHz), as well as with a Bruker
53
54 AMX300 system (300 MHz). The temperature was set to 37 °C for all measurements and a
55
56
57
58
59
60

1
2
3 standard echo time of 1 ms was used. Finally, the relaxivities (r_1 and r_2) were calculated after
4
5 normalization of the relaxation rates ($1/T_1$ and $1/T_2$) to the Gd^{3+} concentration values (as
6
7 measured by ICP-MS).
8

9
10 ***¹⁹F relaxometric properties measurement:*** The fluorine relaxation times (T_1 and T_2)
11
12 were measured with aqueous suspensions containing 10% D_2O . They were acquired at 470.5
13
14 MHz without 1H decoupling on Bruker 500 MHz NMR spectrometer. All measurements were
15
16 performed at 25 °C. T_1 and T_2 were reported for the single fluorine peak at -68.4 ppm. The
17
18 longitudinal relaxation time (T_1) was measured by the standard inversion recovery method,
19
20 and the transverse relaxation time (T_2) was measured by the spin-echo method and the Carr –
21
22 Purcell – Meiboom – Gill (CPMG) pulse sequence. For each measurement, a minimum of 12
23
24 data points were acquired.
25
26

27
28 ***¹⁹F MR Imaging:*** The suspensions of particles were scanned with a 9.4 T animal
29
30 scanner (Varian, Palo Alto, CA) using a transmit-and-receive surface radiofrequency coil. A
31
32 UTE (ultra-short echo time) pulse sequence was used to avoid T_2 signal loss. Pulse sequence
33
34 parameters were as follows: echo time 0.1 ms, repetition time 10 ms, flip angle 6°, 16 signal
35
36 averages, matrix 32x32x32, field of view 30×30×30mm³, and total acquisition time 1h27min.
37
38 The obtained image was interpolated 4 times, and an average of 4 slices was performed in the
39
40 slice dimension, resulting in a slice thickness of 3.75 mm.
41
42
43
44
45

46 47 **RESULTS AND DISCUSSION**

48 49 **1. Synthesis of MSNs, Fluorination and Textural Properties**

50
51 As illustrated in Figure 1, two types of fluorinated nanoparticles were synthesized from pure
52
53 mesoporous silica nanoparticles of the MCM-48 type. In the first functionalization strategy,
54
55 we used a small fluorosilane molecule as the source of fluorine (dimethoxy-methyl(3,3,3-
56
57
58
59
60

1
2
3 trifluoropropyl)silane). This compound contains 3 fluorine atoms per molecule (molecular
4 diagram illustrated in Figure 1). In the second functionalization strategy, the source of
5 fluorine was a polyfluorosiloxane macromolecule (i.e., Poly(methyl-3,3,3-
6 trifluoropropyl)siloxane). This polyfluorosiloxane is a polymer of the fluorosilane molecule (n
7 = 14) and contains 42 fluorine atoms per macromolecule. Its molecular diagram is illustrated
8 in Figure 1.
9
10
11
12
13
14
15

16 In the first functionalization strategy, simple fluorosilane molecules were grafted at the
17 surface of MSNs ("F" = (3,3,3-trifluoropropyl)methyldimethoxysilane; illustrated in Figure 1)
18 However, the first step was the grafting of the DTPA chelation agent to allow the subsequent
19 labeling of paramagnetic Gd^{3+} according to our previous reported work.²⁴ The resulting
20 nanoparticles are referred to as "MSN-DTPA". Then, the nanoparticles were functionalized
21 with fluorosilane, yielding fluorosilane-labeled nanoparticles ("FMSN-DTPA"). Finally, Gd^{3+}
22 was chelated in DTPA, and the resulting fluorinated nanoparticles were designated as
23 "FMSN-DTPA(Gd)".
24
25
26
27
28
29
30
31
32
33

34 In the second functionalization strategy, polyfluorosiloxane molecules were grafted on
35 MSNs ("polyF" = poly(methyl-3,3,3-trifluoropropyl)siloxane; illustrated in Figure 1). These
36 molecules were grafted first, using a thermal immobilization procedure performed at 200 °C
37 and under nitrogen atmosphere. This step led to polyfluorosiloxane-labeled nanoparticles
38 ("polyFMSN"). Then, DTPA molecules were grafted at the surface, yielding
39 polyfluorosiloxane-labeled nanoparticles ("polyFMSN-DTPA"). In order to disperse
40 polyFMSN-DTPA in aqueous media, hydrophilic polyethylene glycol chains (PEG, 20 kDa)
41 were grafted at the surface of this system. Finally, after Gd^{3+} chelation, the resulting
42 fluorinated and PEGylated nanoparticles were designated as polyFMSN-DTPA(Gd)-PEG. For
43 simplified abbreviation, FMSN-DTPA and polyFMSN-DTPA-PEG nanoparticles are simply
44 referred to as FMSNs and polyFMSNs in the following text.
45
46
47
48
49
50
51
52
53
54
55
56
57
58
59
60

1
2
3 Pristine MSNs were visualised by transmission electron microscopy (TEM), which
4 showed well-defined spherical particles of an average particle size of 140 nm (Figure 1-a).
5
6 Low-angle XRD data revealed the typical peaks of the ordered 3-D cubic $Ia\bar{3}d$ mesopore
7 structure (Figure S1-a). This structure is a signature of MSNs belonging to the MCM-48 type.
8
9 N_2 physisorption results showed a type IV isotherm (Figure S1-b), which is associated to the
10 presence of uniform, narrow and cylindrical mesoporous channels. The following values were
11 also extracted from the N_2 physisorption measurements: high specific surface area ($1200 \text{ m}^2 \text{ g}^{-1}$
12 ; using the BET method; see Table 1); large total pore volume ($1 \text{ cm}^3 \text{ g}^{-1}$; NLDFT method;
13 Table 1); mean pore diameter of 3.4 nm (NLDFT method, Table 1 and Figure S1-c).
14
15
16
17
18
19
20
21
22

23 Thermogravimetric analysis of the MSN-DTPA nanoparticles (Figure S2-a) showed a
24 weight loss of 6.3% (i.e. after grafting of DTPA only). For FMSN-DTPA, an additional
25 weight loss of 8.5% was found after fluorosilane grafting. These fractions correspond to the
26 thermal decomposition of DTPA and fluorosilane molecules, respectively. For polyFMSN,
27 the mass percentage (w/w) attributed to polyfluorosiloxane reaches 18% (Figure S2-b). This
28 led to fluorine contents of 0.06 g per gram of polyFMSNs, versus 0.02 g of fluorine per gram
29 of FMSNs. Additional weight losses of 4.3% and 2% were observed on polyFMSN profiles
30 after grafting of DTPA, and PEG, respectively (Figure S2-b). The hydrophobic or hydrophilic
31 character of the MSN surfaces was also evaluated. For this, pure and F-modified nanoparticles
32 were suspended in water and dried at 50 °C overnight before TGA measurement. The initial
33 part of the TGA profiles showed a rapid weight loss of 9.8%, 1% and 0.7% for pure MSNs,
34 FMSNs and polyF-MSNs, respectively. This corresponds to the total evaporation of water
35 molecules physisorbed at the different surfaces of the nanoparticles (both external and inner
36 surfaces).
37
38
39
40
41
42
43
44
45
46
47
48
49
50
51
52
53

54 The characteristics of the porosity were measured after each functionalization step and
55 the data are summarized in Table 1. For fluorosilane-nanoparticles, 100% of the mean pore
56
57
58
59
60

1
2
3 diameter was preserved after DTPA grafting, as well as 90% of both the surface area and the
4
5 pore volume compared to pure MSNs (Table 1). These results suggests that DTPA molecules
6
7 are preferentially grafted at the outer surface of nanoparticles, as reported and demonstrated in
8
9 our previous work.²⁴ After fluorosilane grafting, the specific surface area, the pore volume
10
11 and the pore size decreased to $950 \text{ m}^2 \text{ g}^{-1}$, $0.76 \text{ cm}^3 \text{ g}^{-1}$ and 3 nm, respectively (Table 1). This
12
13 indicated that fluorosilane molecules are grafted at the inner mesopore surface. After
14
15 polyfluorosiloxane functionalization, the specific surface area, the pore volume and the pore
16
17 size were found to be $937 \text{ m}^2 \text{ g}^{-1}$, $0.75 \text{ cm}^3 \text{ g}^{-1}$ and 2.8 nm, respectively (Table 1). This
18
19 suggests the presence of polyfluorosiloxane on the entire exposed MSN surface: external and
20
21 inner surface (i.e., inside the pores and at the entrance of the pores). After DTPA grafting on
22
23 polyFMSNs, a very slight decrease of the surface area and of the pore volume were recorded
24
25 (about 5%, down to $886 \text{ m}^2 \text{ g}^{-1}$; $0.72 \text{ cm}^3 \text{ g}^{-1}$), whereas the mean pore diameter remained
26
27 constant (2.8 nm). The additional grafting of 2% PEG led to a slight decrease (about 15%) of
28
29 the surface area and of the pore volume ($759 \text{ m}^2 \text{ g}^{-1}$ and $0.61 \text{ cm}^3 \text{ g}^{-1}$, respectively). The mean
30
31 pore diameter remained unchanged (2.8 nm). These data suggest that DTPA and PEG were
32
33 localized at the external surface of the nanoparticles. Overall, the porosity data confirm that
34
35 high pore volumes and surface areas are preserved for both systems (FMSNs and
36
37 polyFMSNs). No evidence was found of pore blocking, which is an essential condition for
38
39 considering these imaging probes for future drug delivery applications.
40
41
42
43
44
45

46 2. Spectroscopic Characterisation of FMSNs and polyFMSNs

47
48 For FMSN-DTPA and polyFMSN-DPTA-PEG, the success of molecule grafting was
49
50 confirmed at each step using both solid-state NMR and X-ray photoelectron spectroscopy
51
52 (XPS). Figure 2-a shows the ^{19}F MAS NMR spectra of both types of fluorinated
53
54 nanoparticles. The spectra indicate a single resonance peak at -73 ppm, corresponding to
55
56 $-\text{CF}_3$ species.²⁹ The ^{13}C CP-MAS NMR spectra (Figure 2-b) revealed the resonance peaks
57
58
59
60

1
2
3 characteristic of each carbon atom present in the grafted molecules (DTPA-silane^{24, 25} and
4 fluorosilane molecules²⁹ for FMSN-DTPA nanoparticles; polyfluorosiloxane, DTPA-silane
5 and PEG-silane molecules for polyFMSN-DPTA-PEG nanoparticles). The assignments of
6 each peak are indicated in Figure 2-b. The solid-state ²⁹Si MAS NMR spectra of both
7 fluorinated nanoparticles (Figure 2-c) depicted a broad multicomponent peak in the -88 to -
8 120 ppm range. This contribution correspond to the Q_n groups, n: [1–4], of the silica
9 framework (Si(OSi)_x (OH)_{4-x}; x: [1–3]).^{24, 25} A short-intensity resonance was also found at -
10 54 ppm, which is related to the T₁ groups (C-Si(OSi)₃) of the covalently-grafted DTPA-silane
11 molecules. With respect to the PEG molecules grafted at the surface of MSNs, the
12 corresponding ²⁹Si NMR peak was in the background level. Additional resonances were also
13 observed around [-5 – -24 ppm] for fluorosilane-nanoparticles, corresponding to the D_n
14 groups (R₂-Si(OSi)_n(OR)_{2-n}; n: [1–2]).^{9, 29} This confirms the covalent grafting of fluorosilane
15 molecules at the MSNs surfaces. For polyF-nanoparticles, the ²⁹Si NMR spectra revealed a
16 peak at -22 ppm. This contribution presents a shoulder in the range of [-16 – -19 ppm],
17 indicating the generation of new silicon species either attributed to the resonance of the
18 polyfluorosiloxane backbone (D₂' groups), or to the polyfluorosiloxane group chemically
19 bonded onto the silica particles (D₂ groups),⁹ respectively (Figure 2-c and 2-e).

20
21 XPS detects the presence of elements in a maximum depth of a few nanometers only.
22 In the present study, the particles were XPS-analyzed at each step of the functionalization
23 process, to confirm the element ratios at the surface of nanoparticles. The elemental
24 composition analysis performed before and after DTPA grafting on pristine MSNs (Table 2)
25 showed an increase both in the carbon atomic percentage (%C; up to 10.9%), and in the
26 carbon-to-silicon ratio (C/Si, up to 0.42). High-resolution analysis (HR-XPS) was performed
27 on the C(1s) and on the N(1s) peaks of MSN-DTPA, and this revealed an association between
28 the C(1s) band at 288.8 eV and the appearance of nitrogen (%N = 1.2%). Both bands were
29
30
31
32
33
34
35
36
37
38
39
40
41
42
43
44
45
46
47
48
49
50
51
52
53
54
55
56
57
58
59
60

1
2
3 ascribed to the C=O amide/acid, which is a component of the DTPA molecules. After
4 fluorosilane functionalization of MSNs-DTPA (FMSNs), the atomic percentage of carbon
5 increased by 14.2%, and the carbon-to-silicon ratio (C/Si) also increased up to 0.55 compared
6
7
8
9
10
11
12
13
14
15
16
17
18
19
20
21
22
23
24
25
26
27
28
29
30
31
32
33
34
35
36
37
38
39
40
41
42
43
44
45
46
47
48
49
50
51
52
53
54
55
56
57
58
59
60

ascribed to the C=O amide/acid, which is a component of the DTPA molecules. After fluorosilane functionalization of MSNs-DTPA (FMSNs), the atomic percentage of carbon increased by 14.2%, and the carbon-to-silicon ratio (C/Si) also increased up to 0.55 compared with pristine MSNs. The strong presence of fluorine (%F = 4.5%) was noted, as well as a new C(1s) band appearing at 292.6 eV. This band corresponds to the C atoms linked to F (Table 2). Overall, these results confirmed the presence of DTPA and fluorosilane molecules at the outer surface of the MSNs, following their grafting on pristine nanoparticles.

The presence of DTPA and PEG at the outer surface of polyMSNs was also confirmed by XPS analysis, with high-resolution peaks measured on F(1s), C(1s), N(1s), O(1s) and Si(2s). The grafting of polyfluorosiloxane at the surface of MSNs is reflected by a strong F(1s) peak, as well as by a C(1s) band at 292.6 eV (ascribed to C–F). The atomic percentage of fluorine (%F = 9.7%) is considerably higher than that observed on FMSNs (%F = 4.5%). Significant increase in %C (14%) and C/Si (0.6) ratio were also found after polyfluorosiloxane grafting. This is attributed to the carbon backbone of the polyfluorosiloxane. After the grafting of DTPA, these values reached 16.8% (%C) and 0.75 (C/Si), respectively. The presence of nitrogen was also evidenced from the detection of nitrogen (%N = 0.35) as well as for the presence of the C(1s) bond at 288.8 eV (C=O amide/acid). After PEG grafting, an additional increase of %C and C/Si ratio was evidenced (%C = 18.1%; C/Si = 0.84).

3. Colloidal Stability of FMSNs and polyFMSNs

The measurement of relaxometric properties of fluorinated and paramagnetic contrast agents, requires the precise measurement of ^{19}F and ^1H relaxation times. However, a fundamental prerequisite for this is to demonstrate the colloidal stability of the nanoparticles over time.

1
2
3 The colloidal stability of FMSN-DTPA and polyFMSN-DPTA-PEG suspensions in nanopure
4 water as well as in phosphate-buffered saline (PBS, pH = 7.4), was measured by DLS. The
5 hydrodynamic diameter profiles are shown in Figure 3 (intensity weighted). The
6 hydrodynamic diameter distributions of pristine MSNs, FMSN-DTPA and polyFMSN-
7 DTPA-PEG, were all included in a similar size range, with mean values of $183 - 193 \pm 45$ nm
8 and of $181 - 203 \pm 57$ nm for particles suspended in nanopure water and in PBS,
9 respectively). These values appear higher than the TEM mean particle size, which is expected
10 taking into account the hydration corona around the particles. In addition, a very low
11 polydispersity index (PDI) was obtained (PDI = [0.04 - 0.121] and [0.06 - 0.02] for
12 nanoparticles suspended in water and in PBS, respectively). No evidence was found of
13 agglomeration or flocculation. A robust colloidal stability was found for a period of at least 1
14 week following preparation (Figure 3-a-ii and 3-b-jj).

30 4. ^{19}F Relaxometric Properties of FMSNs and polyFMSNs

31
32 The ^{19}F relaxometric properties of the nanoparticle suspensions were measured by NMR
33 spectroscopy. First, the ^{19}F NMR spectra obtained with FMSN-DTPA colloidal suspensions
34 revealed a single resonance peak at -68.4 ppm. This peak was estimated sufficiently narrow to
35 be useful for detection in the MRI studies planned as next steps of this study (Figure S3-a).
36 The shape of this peak confirms the single chemical environment of ^{19}F nuclei contained in
37 the $-\text{CF}_3$ groups of fluorinated-MSNs samples. Single peaks are ideal for ^{19}F MR imaging
38 applications, since they prevent the occurrence of chemical shift artifacts which are frequent
39 with fluorinated molecules. This effect fractionates the signal, and as a result MRI artefacts
40 can be generated.³⁰ The $-\text{CF}_3$ groups are also very advantageous for *in vitro* and *in vivo* ^{19}F
41 MRI because of their relatively long T_2 , compared to $-\text{CF}_2$ groups present in many
42 perfluorocarbons (e.g., perfluoro-crown-ether, C_6F_6). The relatively long T_2 of $-\text{CF}_3$ groups
43 preserve the attenuation of the MR signal, leading therefore to better ^{19}F MRI detection.³⁰
44
45
46
47
48
49
50
51
52
53
54
55
56
57
58
59
60

1
2
3
4
5 The ^{19}F NMR spectra were integrated over the entire resonance peak, and the data were
6
7 plotted against F concentration to confirm that the signal is directly proportional to the ^{19}F
8
9 content of the suspensions (Figure S3-b). A very high signal-to-noise linearity ratio was found
10
11 ($r^2 = 0.999$). After integration of the total signal intensity, the relaxation times (T_1 and T_2) of
12
13 fluorine were measured. The corresponding relaxation rates R_1 and R_2 ($R_1 = 1/T_1$ and $R_2 =$
14
15 $1/T_2$) were then plotted in function of fluorine concentration. Trifluoroacetic acid (TFA) was
16
17 used as a ^{19}F NMR reference to quantify the concentration of fluorine in the suspensions. This
18
19 measurement revealed a dependence of the relaxation rates on the fluorine concentration, in a
20
21 similar manner as for paramagnetic contrast agents measured in proton (^1H) MRI. Figure 4
22
23 shows the relaxation curves obtained for FMSNs and polyFMSNs. The relaxation curves
24
25 revealed a dependence with the fluorine concentration, $[^{19}\text{F}]$, up to 9 mM: R_1 and R_2 values
26
27 increased with the increase of fluorine concentration. However, a sharper variation of the
28
29 transverse relaxation rate (R_2) was observed (Figure 4-a versus Figure 4-b). This reflects an
30
31 increase of the mutual interactions (i.e. “spin-spin”) between ^{19}F nuclei at higher
32
33 concentrations. In fact, transverse or spin-spin relaxation (T_2) is more affected by fluorine
34
35 concentration than longitudinal, or spin-lattice relaxation (T_1).³⁰ Interestingly, better
36
37 relaxometric properties were obtained with polyFMSNs, compared to FMSNs. The R_1 curve
38
39 of polyFMSNs is slightly above the R_1 curve of FMSNs, indicating similar longitudinal
40
41 relaxivities for both fluorinated nanoparticles (Figure 4-a). However, the R_2 of polyFMSNs
42
43 were significantly lower than that of FMSNs: the slope of the R_2 relaxation curve equals to
44
45 $4.69 \text{ s}^{-1} \text{ mM}^{-1}$ for polyFMSNs versus $14.05 \text{ s}^{-1} \text{ mM}^{-1}$ for FMSNs, respectively (Figure 4-b).
46
47 Hence, the spins of fluorine atoms contained in the relatively long molecular chains of
48
49 polyfluorosiloxane (on polyFMSNs), are less susceptible to influence each other compared
50
51 with the more closely spaced $-\text{CF}_3$ moieties grafted at the surface of FMSNs, which are
52
53
54
55
56
57
58
59
60

1
2
3 grafted with short, less mobile, less flexible molecules. A combination of short T_1 and as long
4
5 T_2 as possible is necessary to allow persistent and high signal in ^{19}F -MRI.

6
7 After chelation of Gd^{3+} by the DTPA attached at the surface of FMSN and
8
9 polyFMSNs, a strong increase in the relaxation rates of ^{19}F nuclei was observed: 3 and 9 times
10
11 higher than that obtained before gadolinium chelation, respectively (Figure S4). This indicates
12
13 that the relaxation of ^{19}F nuclei can be influenced by the presence of gadolinium ions in their
14
15 vicinity. Hence, the strong interactions between the electron spins of the paramagnetic ions,
16
17 and the magnetic moments of the ^{19}F nucleuses, have a dramatic impact on the capacity of
18
19 fluorine to relax its energy. Also, the discrete distribution of Gd ions at the nanoparticle
20
21 surfaces can alter the local magnetic fields, giving gives rise to an inhomogeneous magnetic
22
23 field that affects the dipolar interactions between the ^{19}F nuclei and the Gd^{3+} ions.^{31, 32}
24
25 However, the R_1 and R_2 relaxation rates of ^{19}F do not increase in the same proportion; in fact,
26
27 the much stronger impact on transverse relaxation (R_2) could impede the capacity of the
28
29 contrast agent to produce a strong and lasting ^{19}F MRI signal, as stronger spin-spin
30
31 interactions are more susceptible to cause spin dephasing and ultimately, signal attenuation.
32
33
34
35
36

37 **5. ^1H Relaxometric Properties**

38
39 The ^1H relaxometric properties of FMSN-DTPA(Gd) and polyFMSN-DPTA(Gd)-PEG
40
41 nanoparticles were studied in a large range of magnetic field strengths, from 0.015 to 300
42
43 MHz. Usually, MRI scanners in the clinics operate in the range 1.41 T – 3.0 Tesla (60 – 120
44
45 MHz). Longitudinal (T_1) and transversal (T_2) proton relaxation times were measured. Then,
46
47 the corresponding relaxivity values (i.e., relaxation rates normalized to Gd^{3+} concentration; r_1
48
49 and r_2) were calculated to assess the ^1H relaxometric potential of each type of nanoparticles.
50
51 In order to study the influence of medium viscosity on the ^1H relaxometric properties,
52
53 measurements were performed not only in water, but also with hydrogel-entrapped
54
55 nanoparticles. Nuclear magnetic relaxation dispersion (NMRD) profiles obtained on these
56
57
58
59
60

1
2
3 systems are shown in Figures 5-a and 5-b. Similar profiles were revealed between FMSN-
4 DTPA(Gd) and polyFMSN-DTPA(Gd)-PEG, with nanoparticles either suspended in water or
5 entrapped in hydrogel. The longitudinal relaxivity (r_1) was quite constant at low fields (< 20
6 MHz). Although we cannot rule-out the possible presence of a few detached Gd-DTPA
7 molecules in the samples, the NMRD spectra appear similar to that of Gd-bound large
8 complexes (e.g. Gd-containing proteins, Gd-MSN). They do not present the typical
9 characteristics of Gd-DTPA molecules.³³

10
11
12
13
14
15
16
17
18
19
20
21 At higher fields, r_1 values increase and peak in the range 20 - 60 MHz, followed by a sharp
22 decrease. For the transversal relaxivity (r_2), a sharp increase was noted at higher fields.
23 This shape of NMRD profiles is typical of suspensions of nanoparticles and macromolecules
24 labeled with paramagnetic chelates.^{25, 34, 35} With respect to the suspension medium, at high
25 magnetic field strength (>20 MHz) the longitudinal relaxivity (r_1) of nanoparticles in aqueous
26 suspension was higher than that of nanoparticles entrapped in hydrogel, and this for both
27 types of nanoparticles. In fact, the r_1 values were typically 15 – 2 times higher in this range of
28 magnetic field strengths. Also the maximum peak seems to appear at higher magnetic field for
29 nanoparticles suspended in water (40 – 60 MHz), compared to the particles entrapped in
30 hydrogel (22.7 – 29 MHz). These relaxometric differences are mainly due to the constrained
31 diffusion of water in the hydrogel network. In addition, the longitudinal relaxivity values
32 depend on the correlation time between water ^1H protons and the contrast agent. At high field
33 strengths (> 10-20 MHz), this correlation time is limited either by the exchange correlation
34 time, or by the rotational time.³⁴ Hence, the higher the viscosity of a Gd-nanoparticle contrast
35 media, the longer the exchange correlation time and the longer the rotation time of this
36 compound. Each one of these factors has an impact on the relaxometric performance, and this
37 explains the slightly reduced performance of the contrast agent one entrapped in hydrogel.
38
39
40
41
42
43
44
45
46
47
48
49
50
51
52
53
54
55
56
57
58
59
60

1
2
3 Overall, the relaxivity values of polyFMSN-DPTA(Gd)-PEG were lower compared to
4 the values found for FMSN-DPTA(Gd) (Figure 5-a and 5-b). This is most probably due to the
5 difference in hydrophobicity between both types of nanoparticles. The fluorine content is
6 significantly higher in polyF-MSNs, and this leads to higher hydrophobicity and a relative
7 decrease of the total interactions between water molecules and the paramagnetic cores directly
8 attached to the silica walls. Nevertheless, similar r_2/r_1 ratios were found at clinical magnetic
9 fields for both nanoparticle types (Figure 5-c). In water, values of 1.45 and 1.44 were found
10 for the r_2/r_1 ratios of FMSNs and polyFMSNs, respectively, whereas in the hydrogel, these
11 counterparts were 2.2 and 2.15 (an increase of about 1.5x, see Figure 5-c). It is generally
12 assumed that positive contrast agents must present r_2/r_1 ratios as close as possible to 1 to be
13 considered as efficient MRI signal enhancers. Hence, these results confirm the high potential
14 of both polyFMSN-DPTA(Gd)-PEG and FMSN-DPTA(Gd) as "positive" contrast agents for
15 proton MRI at clinical magnetic field strengths. The slight decrease in relaxometric properties
16 noted for hydrogel-entrapped samples, is not expected to have a strong impact on their
17 performance as "positive" contrast agents.

18
19
20
21
22
23
24
25
26
27
28
29
30
31
32
33
34
35
36 In addition, we studied the impact of temperature on the longitudinal relaxivity (r_1) of
37 nanoparticles suspended in water and in hydrogel. The longitudinal relaxation time (T_1) was
38 measured in a range of 5 °C to 37 °C, and the relaxivities were calculated (Figure 6). A very
39 limited impact of temperature on the relaxometric properties was found for each type of
40 nanoparticles suspended in water. In the hydrogel however, the longitudinal relaxivity (r_1)
41 increased with the temperature. The diffusion of water molecules, the exchange correlation
42 time and the rotational correlation time are all strongly affected by the modulations of solvent
43 viscosity induced by temperature changes. The impact of temperature is thus stronger with
44 hydrogel-entrapped nanoparticle suspensions.

6. Magnetic Resonance Imaging Studies (^1H and ^{19}F MRI)

The signal enhancement from water protons (^1H) was measured in 1.5 Tesla MRI by imaging tubes containing Gd-chelated fluorinated nanoparticles suspended in water (Figure 7-a). The two types of nanoparticles (Gd-labeled FMSNs and Gd-labeled polyMSNs) produce positive contrast enhancement in T_1 -weighted imaging even at very low Gd concentrations ($[\text{Gd}] = 0.04 - 0.05 \text{ mM}$; at least 99% of contrast enhancement was observed).

The generation of ^{19}F -based MR images was also demonstrated. For this, a phantom study was performed using imaging tubes containing FMSNs and polyFMSNs. Both systems were scanned with a 9.4 T animal scanner (Figure 7). Interestingly, the ^{19}F signal of FMSNs was too low to allow efficient image extraction, and this even at high fluorine concentration ($[\text{F}] = 118 \text{ mM}$; $[\text{nanoparticles}] = 100 \text{ mg mL}^{-1}$). This low signal level was mainly attributed to the relatively low fluorine concentration grafted per unit of FMSN. The very short T_2 relaxation time of FMSNs (see section 4) most likely cause rapid signal decay and impedes the detection of enough ^{19}F signal between each one of the MR excitations.

For polyFMSNs on the other hand, ^{19}F MR images were efficiently generated for concentrations of $[\text{F}] = 190 \text{ mM}$, which correspond to a concentration of nanoparticles as high as 60 mg mL^{-1} . The much more efficient signal detection measured with polyFMSNs was attributed to the longer T_2 values (19.4 ms) measured on these suspensions. Finally, the ^{19}F MRI signal from polyFMSNs that were dispersed in NMR tubes of 5 mm diameter, was much more efficiently detected than those suspended in capillary tubes of smaller diameters (e.g. 1 mm diameter, Figure 7). These results are consistent with the fact that for 5 mm diameter NMR tubes, the MRI voxels are completely enclosed within the volume of the tube, whereas for the 1-mm tubes, partial volume effects might decrease the total signal detected per voxel. These results indicate the necessity to concentrate fluorinated nanoparticles up to a certain level to visualize them in MRI voxels (at least 60 mg mL^{-1} for polyFMSNs). In

1
2
3 addition to high fluorine concentration, long spin-spin relaxation time (T_2) must be achieved
4
5 to reach high signals in ^{19}F MRI. In the present study, this was achieved by labeling MSNs
6
7 with polyfluorosiloxane macromolecules.
8
9

10 **CONCLUSION:**

11
12 In conclusion, novel fluorinated mesoporous silica nanoparticles (MSNs) were developed and
13
14 their properties as ^{19}F contrast agents were comprehensively measured. A variant of these
15
16 nanoparticles was also labeled with gadolinium paramagnetic chelates, and was tested for dual
17
18 ^{19}F - ^1H MR imaging. The grafting of polyfluorosiloxane macromolecules demonstrated an
19
20 effective strategy to increase the density of fluorine atoms at the surface of MSNs. This
21
22 grafting procedure had a strong impact on the total signal detected in ^{19}F MRI. The ^{19}F
23
24 relaxation properties were found to be dependent on the fluorine concentration (at least up to
25
26 $[\text{F}] = 9 \text{ mM}$). Similar longitudinal ^{19}F relaxivities were found for FMSNs and polyFMSNs;
27
28 however, the transverse ^{19}F relaxivities were significantly lower for the polyFMSNs. As a
29
30 result, the latter system was more easily detectable and provided stronger signal enhancement.
31
32 Gd-labeled MSNs produce a strong signal in T_1 -weighted ^1H MRI. The presence of Gd at the
33
34 surface of FMSNs was also associated with a significant increase in ^{19}F relaxivities.
35
36 Unfortunately, the stronger impact on transverse relaxivity could impede the possibility of
37
38 detecting these probes. Finally, suspensions of polyFMSNs were imaged in ^{19}F MR images at
39
40 9.4 T. The relaxometric properties of FMSNs and polyFMSNs nanoparticles could be
41
42 exploited further in the design of biomedical objects such as implantable devices for drug
43
44 delivery or other theranostic applications. The dual detection of ^1H and ^{19}F - MRI signal could
45
46 represent an interesting alternative to the use of radioactive molecules in MRI-PET, or in
47
48 MRI-SPECT.
49
50
51
52
53
54
55
56
57
58
59
60

ASSOCIATED CONTENT

Supporting Information: includes powder XRD patterns; N₂ physisorption isotherms; pore size distributions; porosity data; TGA curves; ¹⁹F NMR spectrum of colloidal suspension of fluorinated nanoparticles; ¹⁹F signal-to-noise ratio linearity curve; and ¹⁹F relaxation rates (R₁ and R₂) of nanoparticles before and after gadolinium chelation. This material is available via the Internet at <http://pubs.acs.org>.

AUTHOR INFORMATION

Corresponding Author

*Marc-André Fortin: marc-andre.fortin@gmn.ulaval.ca

*Freddy Kleitz: freddy.kleitz@chm.ulaval.ca

ACKNOWLEDGEMENT

The authors acknowledge the financial support from the National Science and Engineering Research Council (Canada, Discovery grant 355524-2012) and the Fonds Québécois de la Recherche sur la Nature et les Technologies (Team Grant 2013-PR-167010)). The authors would like to thank M. Pierre Audet (Département de Chimie, Université Laval, Quebec) for assistance in ¹⁹F relaxometric measurements. Prof. Matthias Stuber and M. Roberto Colotti (University Hospital of Lausanne, Switzerland) are also acknowledged for access to ¹⁹F MR Imaging and for contributing to image acquisition, respectively. The authors are grateful to Jean Lagueux for contributing to ¹H MRI.

REFERENCES:

- 1
- 2
- 3 1. Wu, S. H.; Mou, C. Y.; Lin, H. P., Synthesis of mesoporous silica nanoparticles.
4 *Chem. Soc. Rev.* **2013**, *42*, 3862-3875.
- 5 2. Huh, S.; Chen, H. T.; Wiench, J. W.; Pruski, M.; Lin, V. S. Y., Controlling the
6 selectivity of competitive nitroaldol condensation by using a bifunctionalized mesoporous
7 silica nanosphere-based catalytic system. *J. Am. Chem. Soc.* **2004**, *126*, 1010-1011.
- 8 3. Florek, J.; Giret, S.; Juere, E.; Lariviere, D.; Kleitz, F., Functionalization of
9 mesoporous materials for lanthanide and actinide extraction. *Dalton Trans.* **2016**, *45*, 14832-
10 14854.
- 11 4. Melde, B. J.; Johnson, B. J.; Charles, P. T., Mesoporous silicate materials in sensing.
12 *Sensors* **2008**, *8*, 5202-5228.
- 13 5. Walcarius, A., Mesoporous materials and electrochemistry. *Chem. Soc. Rev.* **2013**, *42*,
14 4098-4140.
- 15 6. Monton, M. R. N.; Forsberg, E. M.; Brennan, J. D., Tailoring Sol-Gel-Derived Silica
16 Materials for Optical Biosensing. *Chem. Mater.* **2012**, *24*, 796-811.
- 17 7. Mamaeva, V.; Sahlgren, C.; Lindén, M., Mesoporous silica nanoparticles in
18 medicine—Recent advances. *Adv. Drug Deliv. Rev.* **2013**, *65*, 689–702.
- 19 8. Vivero-Escoto, J. L.; Huxford-Phillips, R. C.; Lin, W. B., Silica-based nanoprobe for
20 biomedical imaging and theranostic applications. *Chem. Soc. Rev.* **2012**, *41*, 2673-2685.
- 21 9. Maldaner, L.; Jardim, I., A new thermally immobilized fluorinated stationary phase for
22 RP-HPLC. *J. Sep. Sci.* **2010**, *33*, 174-181.
- 23 10. Shin, J. H.; Privett, B. J.; Kita, J. M.; Wightman, R. M.; Schoenfish, M. H.,
24 Fluorinated xerogel-derived microelectrodes for amperometric nitric oxide sensing. *Anal.*
25 *Chem.* **2008**, *80*, 6850-6859.
- 26 11. Karmouch, R.; Ross, G. G., Superhydrophobic wind turbine blade surfaces obtained
27 by a simple deposition of silica nanoparticles embedded in epoxy. *Appl. Surf. Sci.* **2010**, *257*,
28 665-669.
- 29 12. Cao, L. L.; Jones, A. K.; Sikka, V. K.; Wu, J. Z.; Gao, D., Anti-Icing
30 Superhydrophobic Coatings. *Langmuir* **2009**, *25*, 12444-12448.
- 31 13. Brassard, J. D.; Sarkar, D. K.; Perron, J., Fluorine Based Superhydrophobic Coatings.
32 *Appl. Sci.* **2012**, *2*, 453-464.
- 33 14. Kuwahara, Y.; Maki, K.; Matsumura, Y.; Kamegawa, T.; Mori, K.; Yamashita, H.,
34 Hydrophobic Modification of a Mesoporous Silica Surface Using a Fluorine-Containing
35 Silylation Agent and Its Application as an Advantageous Host Material for the TiO₂
36 Photocatalyst. *J. Phys. Chem. C* **2009**, *113*, 1552-1559.
- 37 15. Kaneda, M. M.; Caruthers, S.; Lanza, G. M.; Wickline, S. A., Perfluorocarbon
38 Nanoemulsions for Quantitative Molecular Imaging and Targeted Therapeutics. *Ann. Biomed.*
39 *Eng.* **2009**, *37*, 1922-1933.
- 40 16. Srinivas, M.; Heerschap, A.; Ahrens, E. T.; Figdor, C. G.; de Vries, I. J. M., F-19 MRI
41 for quantitative in vivo cell tracking. *Trends in Biotechnol.* **2010**, *28*, 363-370.
- 42 17. Ruiz-Cabello, J.; Barnett, B. P.; Bottomley, P. A.; Bulte, J. W. M., Fluorine (F-19)
43 MRS and MRI in biomedicine. *Nmr in Biomed.* **2011**, *24*, 114-129.
- 44 18. Temme, S.; Bonner, F.; Schrader, J.; Fogel, U., 19F magnetic resonance imaging of
45 endogenous macrophages in inflammation. *Wiley Interdiscip. Rev. Nanomed. Nanobiotechnol.*
46 **2012**, *4*, 329-343.
- 47 19. Freire, M. G.; Dias, A. M. A.; Coelho, M. A. Z.; Coutinho, J. A. P.; Marrucho, I. M.,
48 Aging mechanisms of perfluorocarbon emulsions using image analysis. *J. Colloid Interface*
49 *Sci.* **2005**, *286*, 224-232.
- 50 20. Srinivas, M.; Boehm-Sturm, P.; Figdor, C. G.; de Vries, I. J.; Hoehn, M., Labeling
51 cells for in vivo tracking using 19F MRI. *Biomaterials* **2012**, *33*, 8830-8840.
- 52
- 53
- 54
- 55
- 56
- 57
- 58
- 59
- 60

- 1
2
3 21. Chen, S. Z.; Yang, Y. Q.; Li, H. D.; Zhou, X.; Liu, M. L., pH-Triggered Au-
4 fluorescent mesoporous silica nanoparticles for F-19 MR/fluorescent multimodal cancer
5 cellular imaging. *Chem. Commun.* **2014**, *50*, 283-285.
- 6 22. Nakamura, T.; Sugihara, F.; Matsushita, H.; Yoshioka, Y.; Mizukami, S.; Kikuchi, K.,
7 Mesoporous silica nanoparticles for F-19 magnetic resonance imaging, fluorescence imaging,
8 and drug delivery. *Chem. Sci.* **2015**, *6*, 1986-1990.
- 9 23. Pochert, A.; Vernikouskaya, I.; Pascher, F.; Rasche, V.; Linden, M., Cargo-influences
10 on the biodistribution of hollow mesoporous silica nanoparticles as studied by quantitative F-
11 19-magnetic resonance imaging. *J. Colloid Interface Sci.* **2017**, *488*, 1-9.
- 12 24. Bouchoucha, M.; C-Gaudreault, R.; Fortin, M. A.; Kleitz, F., Mesoporous Silica
13 Nanoparticles: Selective Surface Functionalization for Optimal Relaxometric and Drug
14 Loading Performances. *Adv. Funct. Mater.* **2014**, *24*, 5911-5923.
- 15 25. Laprise-Pelletier, M.; Bouchoucha, M.; Lagueux, J.; Chevallier, P.; Lecomte, R.;
16 Gossuin, Y.; Kleitz, F.; Fortin, M. A., Metal chelate grafting at the surface of mesoporous
17 silica nanoparticles (MSNs): physico-chemical and biomedical imaging assessment. *J. Mater.*
18 *Chem. B* **2015**, *3*, 748-758.
- 19 26. Kim, T. W.; Chung, P. W.; Lin, V. S. Y., Facile Synthesis of Monodisperse Spherical
20 MCM-48 Mesoporous Silica Nanoparticles with Controlled Particle Size. *Chem. Mater.* **2010**,
21 *22*, 5093-5104.
- 22 27. Bouchoucha, M.; Cote, M. F.; C-Gaudreault, R.; Fortin, M. A.; Kleitz, F., Size-
23 Controlled Functionalized Mesoporous Silica Nanoparticles for Tunable Drug Release and
24 Enhanced Anti-Tumoral Activity. *Chem. Mater.* **2016**, *28*, 4243-4258.
- 25 28. Thommes, M.; Cychosz, K. A., Physical adsorption characterization of nanoporous
26 materials: progress and challenges. *Adsorption* **2014**, *20*, 233-250.
- 27 29. Boutevin, B.; Guidapietrasanta, F.; Ratsimihety, A.; Caporiccio, G.; Gornowicz, G.,
28 Study of the Alkylation of Chlorosilanes. Part I. Synthesis of Tetra(1H,1H,2H,2H-
29 Polyfluoroalkyl)Silanes. *J. Fluorine Chem.* **1993**, *60*, 211-223.
- 30 30. Sotak, C. H.; Hees, P. S.; Huang, H. N.; Hung, M. H.; Krespan, C. G.; Raynolds, S., A
31 New Perfluorocarbon for Use in F-19 Magnetic-Resonance-Imaging and Spectroscopy. *Magn.*
32 *Reson. Med.* **1993**, *29* (2), 188-195.
- 33 31. Senanayake, P. K.; Kenwright, A. M.; Parker, D.; van der Hoorn, S. K., Responsive
34 fluorinated lanthanide probes for F-19 magnetic resonance spectroscopy. *Chem. Commun.*
35 **2007**, *28*, 2923-2925.
- 36 32. Neubauer, A. M.; Myerson, J.; Caruthers, S. D.; Hockett, F. D.; Winter, P. M.; Chen,
37 J. J.; Gaffney, P. J.; Robertson, J. D.; Lanza, G. M.; Wickline, S. A., Gadolinium-Modulated
38 F-19 Signals From Perfluorocarbon Nanoparticles as a New Strategy for Molecular Imaging.
39 *Magn. Reson. Med.* **2008**, *60*, 1066-1072.
- 40 33. Koenig, S. H.; Baglin, C.; Brown, R. D., Magnetic-field Dependence of Solvent
41 Proton relaxation Induced by Gd³⁺ and Mn²⁺ Complexes. *Magn. Reson. Med.* **1984**, *1*, 496-501.
- 42 34. Faucher, L.; Gossuin, Y.; Hocq, A.; Fortin, M. A., Impact of agglomeration on the
43 relaxometric properties of paramagnetic ultra-small gadolinium oxide nanoparticles.
44 *Nanotechnology* **2011**, *22*, 1-10.
- 45 35. Toth, E.; Helm, L.; Merbach, A. E., Relaxivity of MRI contrast agents. In *Contrast*
46 *Agents I: Magnetic Resonance Imaging*, Krause, W., Ed. Springer-Verlag Berlin: Berlin,
47 2002; Vol. 221, pp 61-101.
- 48
49
50
51
52
53
54
55
56
57
58
59
60

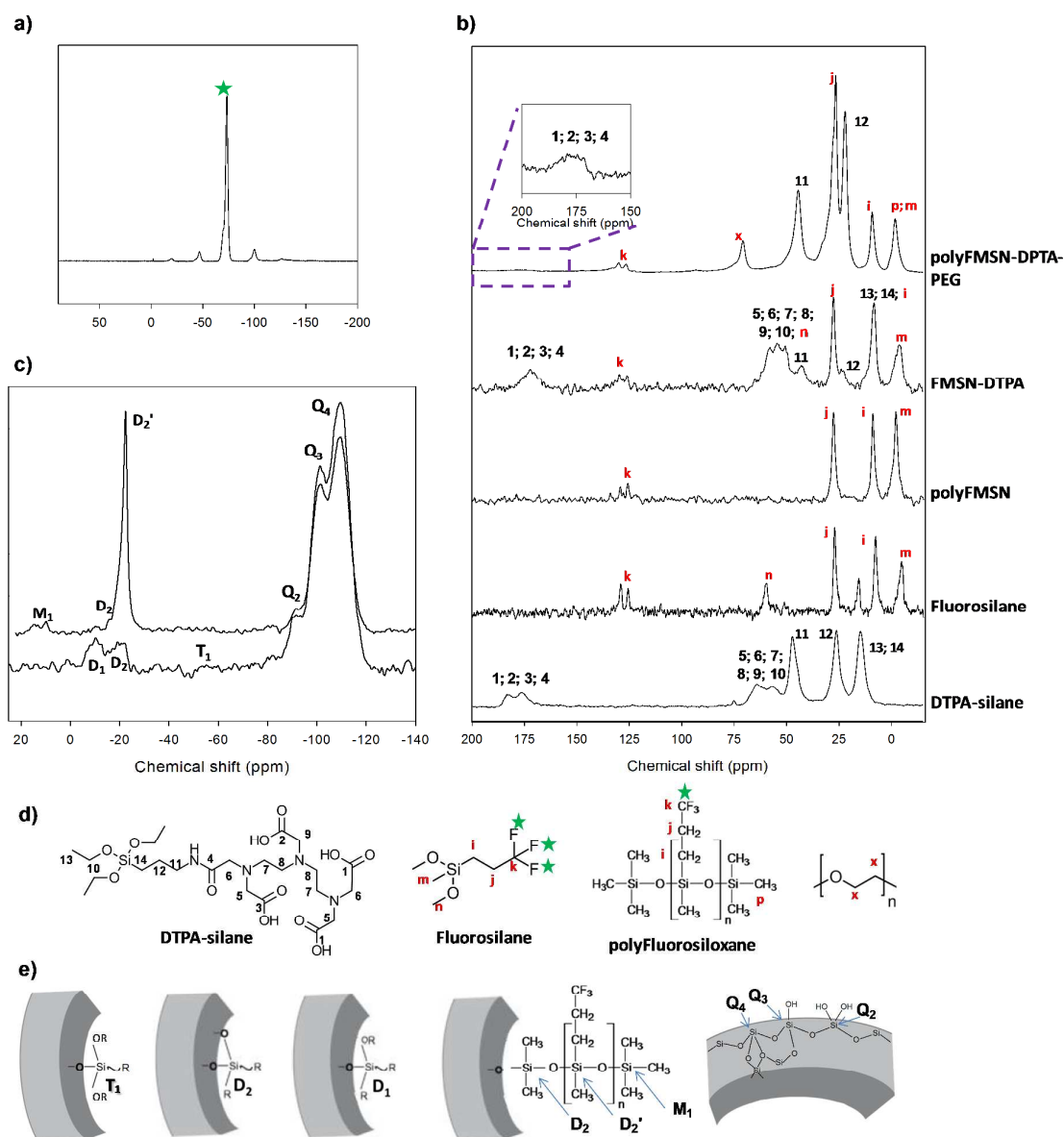


Figure 2. ^{19}F (a), ^{13}C CP (b) and ^{29}Si (c) MAS NMR spectrum of nanoparticles; e) molecular diagrams of DTPA and fluorosilane molecules; d) schematic representations of the surface of nanoparticles after each one of the grafting steps.

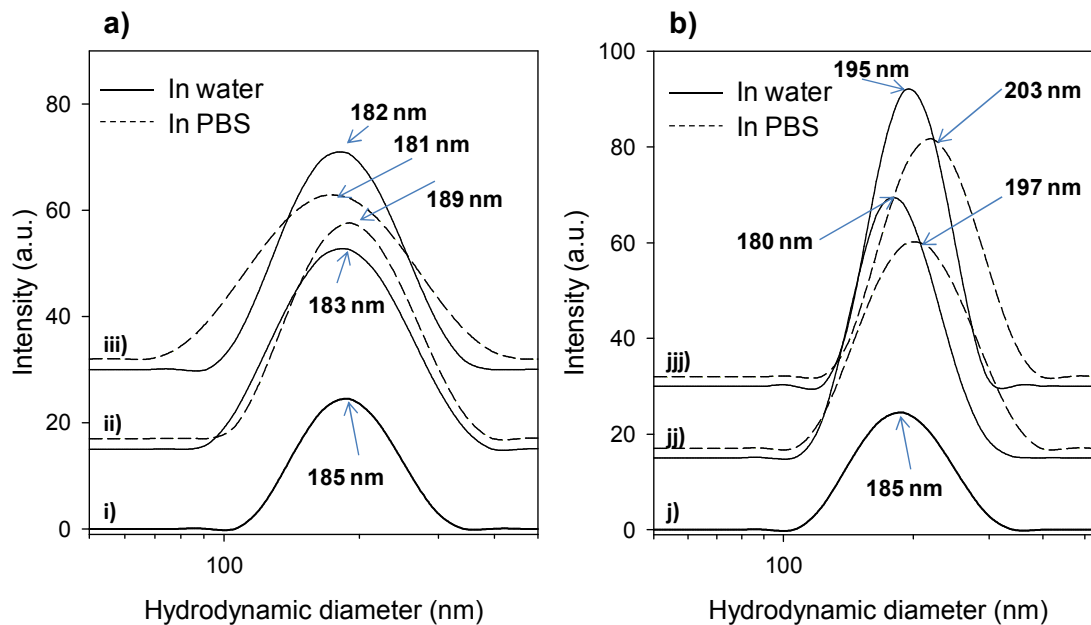


Figure 3. DLS analysis of pure MSNs (a-i and b-j), FMSN-DTPA (a-ii and a-iii) and PolyFMSN-DTPA-PEG (b-ii and b-iii) aqueous suspensions; ii and jj) analysis after 2 h; iii and jii) analysis after 1 week.

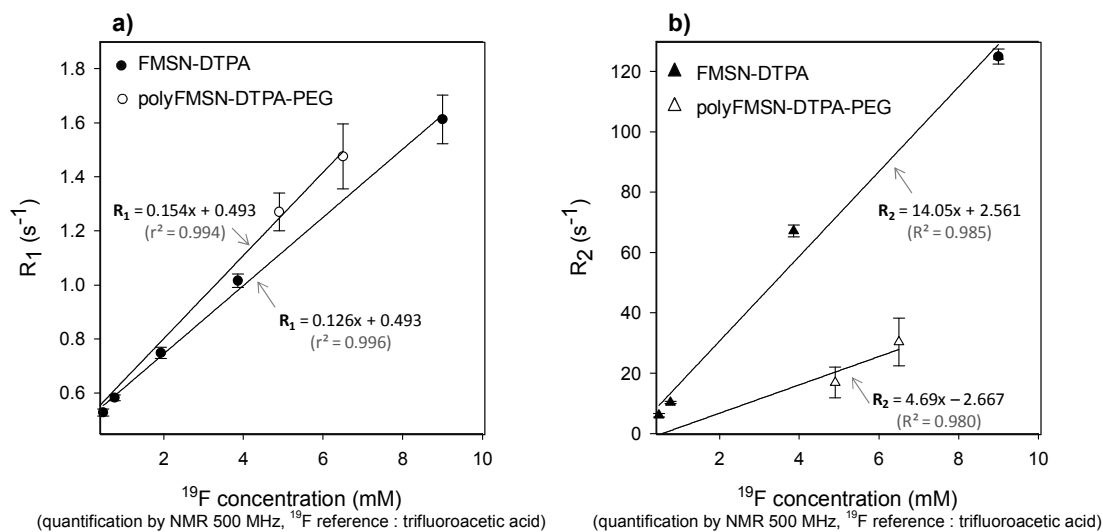


Figure 4. ^{19}F R_1 and R_2 relaxation rates (a and b, respectively) of FMSN-DTPA and polyFMSN-DTPA-PEG nanoparticles measured by NMR spectroscopy.

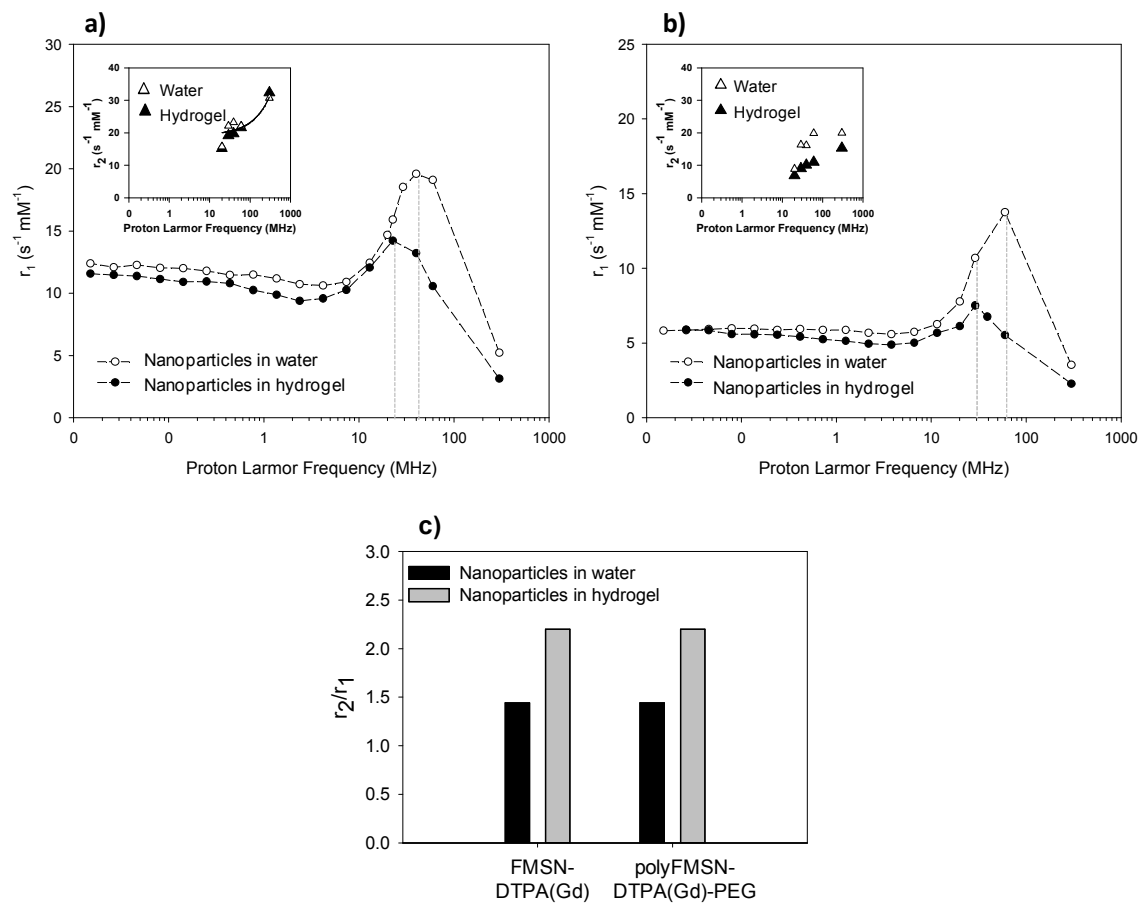


Figure 5. NMRD profiles (r_1 ; r_2 figures in the insets) at variable magnetic field strengths: a) FMSN-DTPA(Gd) ; b) polyFMSN-DTPA(Gd)-PEG suspension. The measurements were performed at 37 °C. c) Comparison of relaxivity ratios (r_2/r_1) measured at clinical magnetic field strengths (1.4 T, 60 MHz, 37 °C).

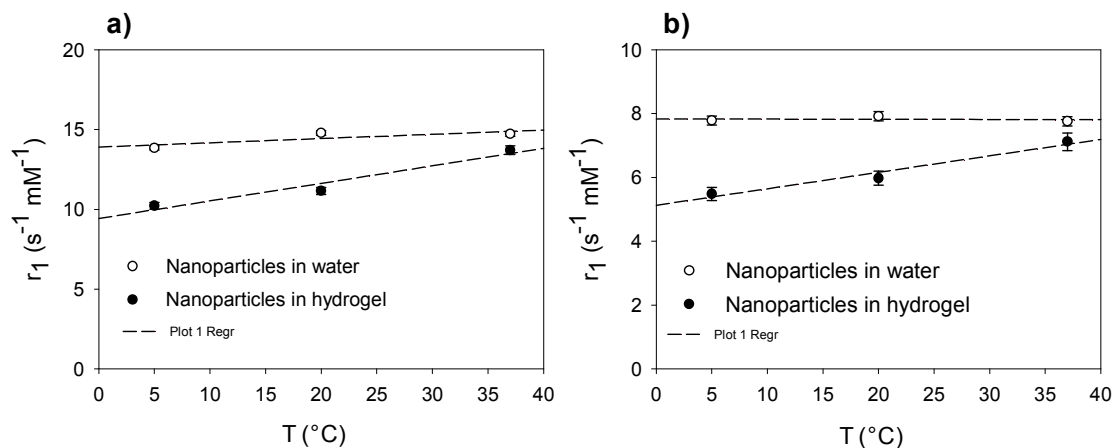


Figure 6. Influence of temperature on the longitudinal relaxivity (r_1) of FMSN-DTPA(Gd) nanoparticles (b) and polyFMSN-DTPA(Gd)-PEG nanoparticles (c) suspended in water and in hydrogel, measured at 20 MHz. For each temperature, the mean value of 3 measurements is represented with a standard deviation included between 1% and 3%.

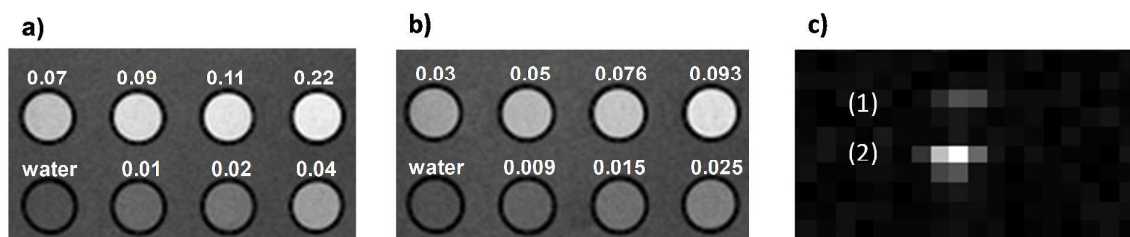


Figure 7. T_1 -weighted ^1H MR images of FMSN-DTPA(Gd) suspensions (a) and polyFMSN-DTPA(Gd)-PEG suspensions (b), measured at clinical magnetic field strength (1.5 Tesla, TE/TR = 10.8/1000 ms). Numerical values indicate the Gd concentrations measured by ICP-MS (in mM). c) ^{19}F MR phantom images of polyFMSN-DTPA(Gd)-PEG nanoparticles acquired in a 9.4 T scanner using an experimental ultra-short echo time sequence. The particles were suspended in a capillary tube of diameter of 1 mm (1) and in a NMR tube of 5 mm (2). Both capillaries appear clearly visible at a low in-plane resolution of $0.94 \times 0.94 \text{ mm}^2$.

TABLES.

Sample	Description	BET Surface Area [m ² g ⁻¹]	Pore Volume [cm ³ g ⁻¹]	NLDFT Mean Pore size [nm]
MSN	MCM-48 (pristine)	1254	0.95	3.4
MSN-DTPA	MCM48-6.3%DTPAsilane	1190	0.91	3.4
FMSN-DTPA	MCM48-8.5%Fluorosilane	950	0.76	3.0
polyFMSN	MCM48- 18%polyFlurosiloxane	937	0.75	2.8
polyFMSN-DTPA	MCM48- 18%polyFlurosiloxane- 4.3%DTPA	886	0.72	2.8
polyFMSN-DTPA- PEG	MCM48- 18%polyFlurosiloxane- 4.3%DTPA-2%PEG	759	0.61	2.8

Table 1. Porosity data of MSNs extracted from nitrogen physisorption measurements.

	% C (1s) (285.2 eV; C-C, C-H) [286.5 eV; C-O, C-N] {289.1 eV; C=O Amide/Acid} <292.8 eV; C-F (CF ₃)>	% N (1s) 399.8 eV; N-H	% O (1s) 532.5 eV	% Si (2s) 103.8 eV; Si-O	% F (1s)	C/Si	F/Si
MSN: MCM-48 (pristine)	1.0 (0.2) [0.8] {-} <->	-	68.5	30.5	-	0.003	-
MSN-DTPA	10.9 (7.35) [2.47] {1.07} <->	1.2	62.1	25.8	-	0.42	-
FMSN-DTPA	14.2 (8.51) [3.18] {1.04} <1.47>	1.0	54.7	25.6	4.5	0.55	0.18
polyFMSN	14.0 (9.19) [1.65] {-} <3.16>	-	53.0	23.4	9.7	0.60	0.41
polyFMSN-DTPA	16.8 (11.47) [3.58] {0.14} <1.61>	0.35	51.4	22.4	9.05	0.75	0.4
polyFMSN-DTPA- PEG	18.1 (11.32) [4.66] {0.30} <1.71>	0.2	51.7	21.6	8.4	0.84	0.39

Table 2. Atomic concentrations (percentages) at the surface of MSNs; data extracted from XPS measurements.

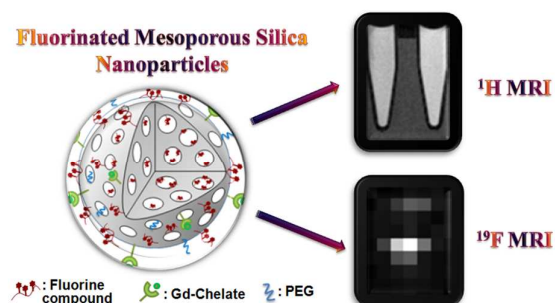


Table of Contents artwork